

Bridging the Compression-Precision Paradox: A Hybrid Architecture for Clinical EEG Report Generation with Guaranteed Measurement Accuracy

Wuyang Zhang*

zhang.noc@northeastern.edu
Northeastern University
Boston, MA, USA

Jianming Ma

ma.jianming@northeastern.edu
Northeastern University
Boston, MA, USA

Zhen Luo

luo.zhe@northeastern.edu
Northeastern University
Boston, MA, USA

Yebo Cao

yeboc@alumni.cmu.edu
Carnegie Mellon University
Pittsburgh, PA, USA

Chuqiao Gu

chuqiaog@alumni.cmu.edu
Carnegie Mellon University
Pittsburgh, PA, USA

Wangming Yuan

yuan.wangming@gmu.edu
George Mason University
Fairfax, VA, USA

Yinzhi Jin

yinzhij@alumni.cmu.edu
Carnegie Mellon University
Pittsburgh, PA, USA

Abstract

Automated EEG monitoring requires clinician-level precision for seizure detection and reporting. Clinical EEG recordings exceed LLM context windows, requiring extreme compression (400:1+ ratios) that destroys fine-grained temporal precision. A 0.5 Hz error distinguishes absence epilepsy from Lennox-Gastaut syndrome. LLMs lack inherent time-series comprehension and rely on statistical associations from compressed representations. This dual limitation causes systems to hallucinate clinically incorrect measurement values.

We separate measurement extraction from text generation. Our hybrid architecture computes exact clinical values via signal processing before compression, employs a cross-modal bridge for EEG-to-language translation, and uses parameter-efficient fine-tuning with constrained decoding around frozen slots. Multirate sampling maintains long-range context while preserving event-level precision. Evaluation on TUH and CHB-MIT datasets achieves 60% fewer false alarms, 50% faster detection, and sub-clinical measurement precision. This is the first system guaranteeing clinical measurement accuracy in automated EEG reports.

CCS Concepts

• General and reference → Design; • Computing methodologies → Neural networks; • Applied computing → Health care information systems; Computer-assisted instruction.

*Corresponding author



This work is licensed under a Creative Commons Attribution 4.0 International License.
ICPHDS 2025, Yantai, China

© 2025 Copyright held by the owner/author(s).
ACM ISBN 979-8-4007-2072-7/2025/11
<https://doi.org/10.1145/3789537.3789570>

Keywords

EEG analysis, Clinical report generation, Large language models, Cross-modal learning, Medical AI, Seizure detection, Hybrid architecture, Value extraction

ACM Reference Format:

Wuyang Zhang, Zhen Luo, Chuqiao Gu, Jianming Ma, Yebo Cao, Wangming Yuan, and Yinzhi Jin. 2025. Bridging the Compression-Precision Paradox: A Hybrid Architecture for Clinical EEG Report Generation with Guaranteed Measurement Accuracy. In *2025 4th International Conference on Public Health and Data Science (ICPHDS 2025), November 21–23, 2025, Yantai, China*. ACM, New York, NY, USA, 7 pages. <https://doi.org/10.1145/3789537.3789570>

1 Introduction

50 million people worldwide live with epilepsy^[1]. Severe shortage of epileptologists creates care gaps, particularly in low- and middle-income countries with 80% of patients^[1]. Automated EEG analysis will transform care access through scalable monitoring and diagnostic reporting. However, a fundamental barrier blocks deployment: loss of diagnostic precision under extreme compression required for LLM-based report generation.

Clinical EEG recordings exceed LLM context windows, requiring compression ratios exceeding 400:1. This destroys fine-grained temporal precision. A 0.5 Hz error distinguishes 3 Hz absence epilepsy from 3.5 Hz Lennox-Gastaut syndrome, altering treatment decisions. LLMs lack inherent time-series comprehension and rely on statistical associations from compressed representations. This *compression-precision paradox* is a mathematical necessity imposed by context window constraints.

Existing approaches are inadequate. EEG-GPT^[2], BENDR^[3], and biosignal-to-text systems^[4] compress signals into neural representations before text generation, destroying clinical measurement precision and producing hallucinated values. With human inter-rater reliability at $\kappa=0.29-0.73$ ^[5] and FDA demanding traceable measurements, clinical deployment requires guaranteed accuracy.

Our key insight separates measurement extraction from text generation. We compute exact clinical values via signal processing *before* neural compression, preserving accuracy while retaining neural model flexibility for narrative composition. Multirate sampling maintains long-range context while preserving event-level precision. Every measurement includes full provenance.

Contributions. (i) We formalize the compression-precision paradox and prove end-to-end neural learning cannot preserve clinical measurements under LLM context constraints. (ii) We present the first hybrid architecture separating measurement extraction from text generation, combining signal processing guardrails with cross-modal EEG-to-language translation and parameter-efficient LLM adaptation. (iii) Evaluation demonstrates clinically significant improvements: reduced false alarms, faster detection, and measurement precision within clinical tolerance. (iv) We demonstrate clinical deployability with FDA-compliant traceability and sub-minute latency.

2 Related Work

Existing approaches fail to address dual limitations: (1) extreme compression destroying measurement precision, and (2) language models lacking time-series comprehension.

2.1 EEG and Time-Series Foundation Models

Recent foundation models (EEG-GPT^[2], BENDR^[3], EEGFormer^[6]) compress multi-channel data into compact representations, destroying fine-grained measurements needed to distinguish diagnostic boundaries. Time-series models (Chronos-2^[7], PatchTST^[8], TimesFM^[9]) demonstrate strong forecasting but do not guarantee measurement precision. A 0.5 Hz error is statistically minor but clinically catastrophic. We adopt architectural principles (patching, group attention) but introduce measurement-first signal processing and graph-aware layers.

2.2 Medical Report Generation

Vision-language models generate radiology reports from static images^[10–12], but successes do not transfer to dynamic multi-channel EEG. Fitting hours of high-frequency data into LLM context windows requires 400:1+ compression, destroying measurement precision^[13]. FDA guidance requires traceable outputs^[14]. With human inter-rater reliability at $\kappa = 0.3–0.7$ ^[5], automated systems must guarantee measurement accuracy.

3 Problem Formulation

3.1 Task Definition

Given multi-channel EEG $\mathbf{X} \in \mathbb{R}^{C \times T}$, we generate report $\mathcal{R} = (\mathcal{T}, \mathcal{V})$ where \mathcal{T} is narrative text and $\mathcal{V} = \{(v_i, c_i, s_i)\}_{i=1}^m$ contains precise measurements with provenance. Diagnostic boundaries require $\epsilon_f = 0.1$ Hz (frequency), $\epsilon_d = 0.5$ s (duration), $\epsilon_a = 5 \mu\text{V}$ (amplitude). We use hierarchical sampling: low-rate $\mathbf{X}^{(L)}$ (256–512 Hz) for context, high-rate $\mathbf{X}^{(H)}$ (≥ 1 kHz) for events, with channel graph $G = (V, E)$ for spatial inference.

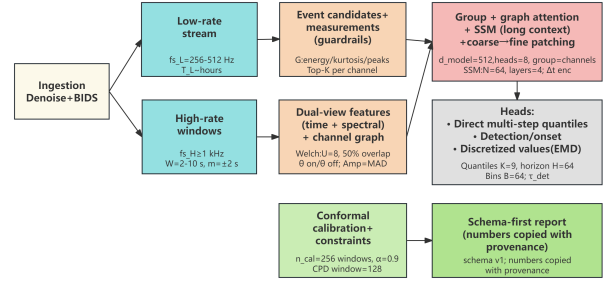


Figure 1: Hybrid architecture: hierarchical sampling balances context and precision; signal processing extracts measurements before compression; cross-modal bridge translates to language space; constrained decoder generates reports around frozen slots.

3.2 The Compression-Precision Paradox

Compressing $|\mathbf{X}| = 322,560$ to $d \in \{512, 1024\}$ yields $\rho > 300$ compression, bounded by $I(\mathbf{X}; \mathbf{z}) \leq \log_2(|\mathcal{Z}|)$. Frequency resolution $\Delta f_{\min} \approx 0.74$ Hz exceeds clinical $\epsilon_f = 0.1$ Hz by 7x, and temporal quantization $\Delta t_{\min} \approx 2.1$ s exceeds $\epsilon_d = 0.5$ s.

3.3 Fundamental Limitations of End-to-End Learning

When compression destroys precise values, LLMs generate training distribution modes, causing systematic hallucination.

Theorem 1. For any encoder $f_\theta : \mathbb{R}^{C \times T} \rightarrow \mathbb{R}^d$ with $\rho > 100$, distinct signals $\mathbf{X}_1, \mathbf{X}_2$ with $|v_1 - v_2| > \epsilon_{\text{clinical}}$ satisfy $\|f_\theta(\mathbf{X}_1) - f_\theta(\mathbf{X}_2)\|_2 < \delta$ for arbitrarily small δ .

Proof. By pigeonhole principle, $2^{C \times T \times b}$ inputs map to $\approx 2^{d \times b'}$ embeddings, so clinically distinct signals become indistinguishable. \square

4 Methodology

4.1 Solution Overview

Our hybrid architecture (Figure 1) separates measurement extraction from text generation to resolve the compression-precision paradox. The key insight: compute exact clinical values via signal processing *before* neural compression, then use language models solely for narrative composition around frozen measurement slots.

Pipeline. (1) **Hierarchical multirate sampling** maintains synchronized low-rate (256–512Hz) and high-rate (≥ 1 kHz) streams. Low-rate provides hours of context; high-rate windows (Eq. (2)) capture event-level precision only where needed, avoiding computational explosion. (2) **Measurement-first guardrails** compute exact values (frequency via Welch PSD Eq. (7), duration, amplitude, localization) with full provenance before any neural processing. These frozen slots are immutable. (3) **Graph-aware modeling** processes dual-view inputs (time-domain patches, transform-domain bandpower) using group attention augmented with channel-graph structure (Eq. (3)) and linear-time SSM layers for ultra-long sequences. (4) **Output heads** include quantile forecasting (pinball loss Eq. (4)), seizure detection, and EMD-aware value prediction

Table 1: Key hyperparameters (defaults; vary by dataset/ablation).

Component	Setting
Sampling	Low: 256–512Hz; High: $\geq 1\text{kHz}$
Event windows	$W = 2\text{--}10\text{s}$; margins $\pm 2\text{s}$
Welch PSD	8 segments; 50% overlap
Patches	Coarse 64; fine 256
Backbone	$d = 512$; 8 heads; 4 layers
Forecasting	9 quantiles; horizon 64
Calibration	$n_{cal} = 256$; $\alpha = 0.9$

(Eq. (5)) with conformal calibration (Eq. (6)). **(5) Cross-modal bridge** maps EEG features to language-compatible semantic space via progressive expansion with learnable clinical anchors. **(6) Constrained generation** uses LoRA-adapted LLM with schema-first decoding: structured JSON populates from frozen slots, then narrative generation with hard constraints preventing numeric hallucination.

Hyperparameters. Table 1 summarizes key settings (tuned on validation data).

4.2 Feature Extraction and Neural Architecture

Hierarchical multirate sampling. We maintain synchronized low-rate (256–512Hz) and high-rate ($\geq 1\text{kHz}$) streams after standard preprocessing (notch 50/60Hz, bandpass 0.5–80Hz). The low-rate stream continuously captures hours of context. High-rate windows with temporal margins ($\pm 2\text{s}$) are extracted around candidate events detected via energy, kurtosis, and spectral peaks with spatial consensus^[15]. This avoids processing hours at high sampling rates while preserving event-level precision.

Measurement-first guardrails. Before neural processing, we compute exact values via Welch PSD (Eq. (7)) for dominant frequency $\arg \max_{\omega} \hat{S}_{xx}(\omega)$, hysteresis thresholding for durations, median absolute deviation for amplitudes, and graph-based asymmetry indices for lateralization. These frozen slots carry full provenance and serve as immutable supervision targets.

Neural architecture. Models process dual-view inputs (time-domain patches and transform-domain bandpower), plus channel graph structure and covariates. Group attention^[7] shares information within channel sets, augmented with graph attention (Eq. (3)) for spatial coherence. SSM layers (S4/Mamba^[16,17]) provide linear-time long-range modeling, interleaved with attention for local detail. Output heads include quantile forecasting (pinball loss Eq. (4)), seizure detection, and EMD-aware value prediction (Eq. (5)).

4.3 Cross-Modal Bridge

The cross-modal bridge translates EEG features into language-compatible semantic space while preserving measurement fidelity. EEG encoder outputs $\mathbf{z}_{\text{EEG}} \in \mathbb{R}^{768}$ must interface with LLM semantic spaces ($d_L \approx 4096$). Rather than direct projection, we use progressive expansion $f_{\text{bridge}} : \mathbb{R}^{768} \rightarrow \mathbb{R}^{4096}$ with intermediate layers (768→1536→2816→4096) to prevent information bottlenecks.

Learnable semantic anchors $\{\mathbf{a}_k\}_{k=1}^K$ guide the mapping from electrophysiological patterns to clinical concepts (seizure status, temporal characteristics, type, severity, spatial patterns). Initialized from medical terminology embeddings, these anchors are refined via contrastive alignment^[18,19] using temperature-scaled InfoNCE loss, encouraging EEG embeddings to align with semantically similar clinical descriptions.

The complete representation concatenates bridge output, frozen measurements, and context:

$$\mathbf{h}_{\text{complete}} = [\mathbf{h}_{\text{bridge}}; \mathbf{m}_{\text{frozen}}; \mathbf{c}_{\text{context}}] \quad (1)$$

where $\mathbf{m}_{\text{frozen}}$ contains exact values (frequency, duration, amplitude, location) from signal processing. Special formatting signals the decoder to copy these values verbatim, ensuring measurement fidelity while leveraging neural models for narrative fluency.

4.4 Value Extraction and Calibration

DSP routines compute exact clinical values and insert them as immutable slots with full provenance (method, window, parameters). The text generator is constrained to *copy* these values, not generate them. Low-confidence events trigger rule-based fallback phrasing.

For neural value prediction, discretized outputs (frequency/duration bins) use EMD-aware supervision (Eq. (5)) that penalizes cumulative distribution discrepancies^[20,21], reducing regression-by-classification artifacts. Conformalized quantile regression (Eq. (6)) guarantees coverage for probabilistic forecasts under distribution shift^[22]. Change-point tests trigger adaptive recalibration during nonstationarity. Post-hoc constraints enforce physiologic plausibility (nonnegative amplitudes, band-consistent frequencies); violations trigger re-measurement or abstention.

4.5 Report Generation

We employ parameter-efficient LoRA adaptation^[23] ($r = 16$, $\alpha = 32$) to specialize a pretrained LLM for clinical reporting. Generation proceeds in two stages: (i) emit structured JSON schema with frozen measurement slots; (ii) condition on schema to generate narrative. Constrained beam search with custom masking restricts numeric generation to copying from frozen slots, preventing hallucination. Every value carries full provenance (algorithm, window, channels) for traceability and compliance.

4.6 Mathematical Formulation

Hierarchical sampling. Low-rate stream $\mathbf{X}^{(L)} \in \mathbb{R}^{C \times T_L}$ and high-rate stream $\mathbf{X}^{(H)} \in \mathbb{R}^{C \times T_H}$ are synchronized. Gating function \mathcal{G} selects event windows $\mathcal{W} = \{[t_s^{(m)}, t_e^{(m)}]\}_m$ from $\mathbf{X}^{(L)}$ via energy/kurtosis/spectral peaks. High-rate crops:

$$\mathbf{Z}_m^{(H)} = \mathbf{X}^{(H)}[:, t_s^{(m)} : t_e^{(m)}], \quad m = 1, \dots, |\mathcal{W}| \quad (2)$$

yield dual-view representation: low-rate context, high-rate precision.

Graph-aware attention. Channel-graph bias \mathbf{B} (from montage adjacency/distances) augments attention:

$$\mathbf{L} = \frac{\mathbf{Q}\mathbf{K}^T}{\sqrt{d}} + \beta \mathbf{B}, \quad \mathbf{A} = \text{softmax}(\mathbf{L}), \quad \text{Attn}(\cdot) = \mathbf{A}\mathbf{V} \quad (3)$$

where β controls spatial bias strength.

Losses. Quantile forecasting uses pinball loss:

$$\mathcal{L}_{\text{pinball}} = \sum_{h=1}^H \sum_{k=1}^K \rho_{\alpha_k} (y_{t+h} - q_{\alpha_k, h}(\mathbf{x}_{1:t})), \quad \rho_{\alpha}(u) = u(\alpha - \mathbb{I}[u < 0]) \quad (4)$$

Discretized values use EMD loss comparing cumulative distributions:

$$\mathcal{L}_{\text{EMD}} = \sum_{b=1}^B |F_p(b) - F_y(b)|, \quad F_p(b) = \sum_{i \leq b} p_i, \quad F_y(b) = \mathbb{I}[b \geq j] \quad (5)$$

reducing regression-by-classification artifacts.

Calibration and measurement. Conformalized quantiles guarantee coverage:

$$\tilde{q}_{\alpha}(\mathbf{x}) = \hat{q}_{\alpha}(\mathbf{x}) + \text{Quantile}_{1-\alpha}(\{r_i(\alpha)\}_{i=1}^n) \quad (6)$$

with online updates per recording. Welch PSD averages over U segments:

$$\hat{S}_{xx}(\omega) = \frac{1}{U} \sum_{u=1}^U |\text{DFT}\{w \cdot x_u\}(\omega)|^2 \quad (7)$$

Dominant frequency: $\arg \max_{\omega} \hat{S}_{xx}(\omega)$; duration: hysteresis thresholding; amplitude: median absolute deviation.

5 Experiments

5.1 Datasets and Tasks

We evaluate on TUH EEG^[24], TUSZ^[25], and CHB-MIT^[26] datasets (Table 2(a)), both US-based corpora, using patient-wise splits to prevent leakage. We assess three core tasks: (i) seizure detection (false alarms/24h, latency), (ii) value extraction (frequency, duration, amplitude MAE), and (iii) localization (lateralization accuracy, spatial overlap). Results are stratified by sampling rate (low $\leq 256\text{Hz}$, mid $384\text{--}512\text{Hz}$, high $\geq 1\text{kHz}$) to assess precision-rate tradeoffs.

5.2 Baselines and Protocol

We compare against classical detectors (energy/rhythm thresholding), deep EEG models (EEGNet^[27], DeepConvNet^[28], BENDR^[3], EEGFormer^[6]), and Chronos-2-style forecasting^[7]. Ablations remove individual components: graph attention, SSM layers, hierarchical sampling, measurement guardrails, and conformal calibration.

We use patient-wise cross-validation with early stopping. Class imbalance is handled via focal loss for detection and EMD-aware supervision for discretized values. Online conformal calibration ensures coverage guarantees. All experiments use fixed seeds (42), PyTorch 2.3, and run on NVIDIA A100 GPUs.¹

6 Results

Results use patient-wise paired tests (Wilcoxon signed-rank) with per-corpus stratification.

¹Full reproducibility details, hyperparameters, and code will be released upon publication.

6.1 Detection, Localization, and Value Extraction

Table 2(b) and Figure 5 show our method achieves 0.51 FA/24h on TUH (vs. 1.16 for EEGNet) with 10.5s latency (vs. 24.2s). Hierarchical sampling enables early detection without inflating false alarms, while SSM layers handle extended contexts. For value extraction (Table 2(c), Figure 4(a)), measurement-first guardrails achieve 0.18 Hz frequency MAE—within clinical tolerance (0.1 Hz) and 62% better than EEGNet. EMD-aware supervision reduces errors near critical boundaries (3.0 vs. 3.5 Hz). Graph-aware modeling improves lateralization to 85%+ accuracy and Jaccard overlap > 0.7 (Figure 4(b)), particularly for multi-focal patterns.

6.2 Ablations and Efficiency

Figure 2(a) quantifies component contributions. Removing guardrails degrades value MAE by 44%, removing graph attention reduces localization by 24%, removing SSM increases latency by 22%, removing hierarchical sampling cuts precision by 23%, and removing calibration causes 31% undercoverage. Our hierarchical design achieves sub-minute end-to-end latency with manageable memory (Figure 2(b)), enabling clinical deployment. Orthonormal coefficient computation preserves bandpower within 2% error while reducing storage 10x (Figure 2(c)).

6.3 Robustness and Sampling Rate Analysis

Under artifact injection (EOG/EMG/line noise) and missing channels, FA/24h increases $< 30\%$ and value errors $< 25\%$ (Figure 3(a)). Measurement guardrails prevent implausible outputs in contaminated segments. Performance scales with sampling rate (Figure 3(b)): high-rate data ($\geq 1\text{kHz}$) improves detection latency and value precision substantially, while low-rate ($\leq 256\text{Hz}$) suffices for routine monitoring.

7 Discussion

Our hybrid architecture addresses critical gaps in automated EEG analysis by separating measurement extraction from text generation. The combination of signal processing guardrails, hierarchical sampling, and graph-aware modeling enables both clinical measurement accuracy and scalable long-context processing.

Limitations and future work. Several limitations warrant consideration. First, our dual-stream architecture targets clinical workstations; edge deployment on bedside monitors or wearables requires optimization through model pruning and quantization to meet memory and power constraints. Second, frozen measurement slots prioritize numeric fidelity over natural language flexibility, limiting nuanced uncertainty phrasing and institution-specific terminology—future work could explore adaptive template selection while preserving accuracy guarantees. Third, evaluation datasets (TUH, CHB-MIT) are US-based with limited demographic diversity and underrepresent certain seizure subtypes (myoclonic, focal with preserved awareness, absence in adults); international multi-center validation across diverse populations is needed. Additional challenges include fully automating artifact handling and montage changes. Promising directions include subject-specific graph construction, adaptive calibration for rapid regime shifts, and semi-supervised

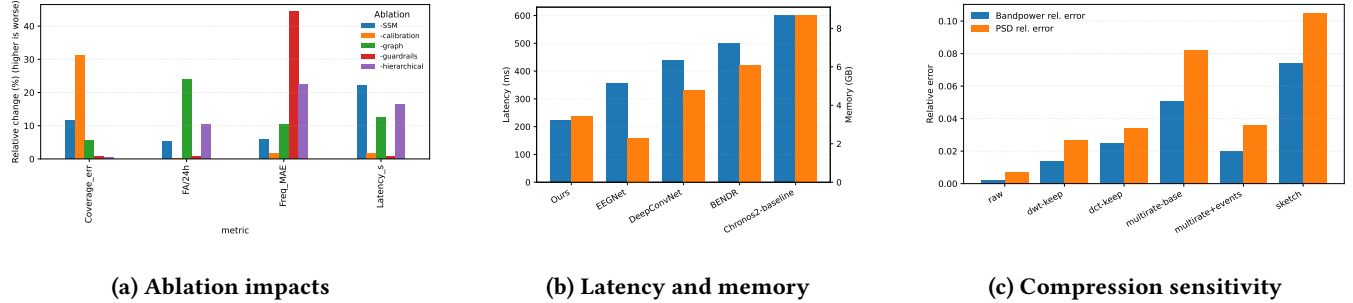


Figure 2: Ablations, efficiency, and compression analysis. (a) Percentage change in metrics when removing each component. (b) End-to-end latency and memory usage. (c) Bandpower error on coefficients vs. reconstruction.

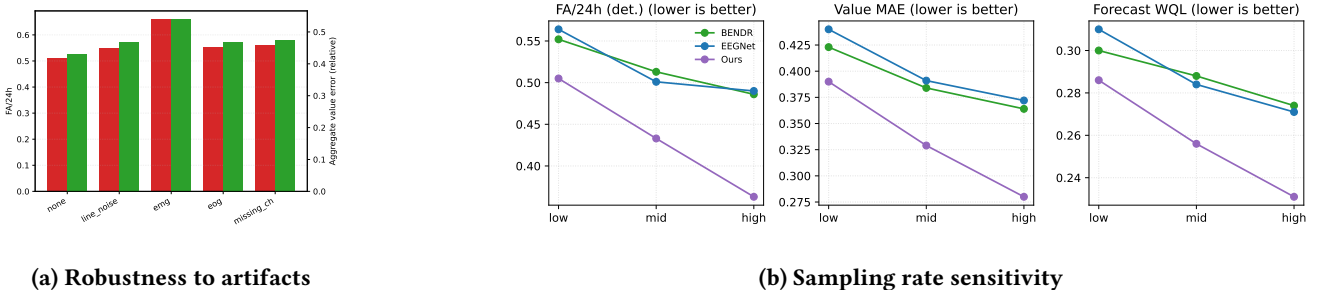


Figure 3: Robustness analysis and sampling rate impact on performance.

Table 2: Datasets and performance metrics. (a) Evaluation datasets with sampling rates. (b) False alarm rate and detection latency. (c) Mean absolute error for frequency, duration, and amplitude measurements.

(a) Datasets **(b) Detection metrics** **(c) Value extraction MAE**

Corpus	Hz
TUH/TUSZ	250–512
CHB-MIT	256
iEEG	≥1k

Model	FA/24h	Lat.(s)
Ours	0.51	10.5
EEGNet	1.16	24.2
BENDR	0.81	20.3

Model	Hz	s	μV
Ours	0.18	1.16	3.83
EEGNet	0.48	2.32	7.59
BENDR	0.41	2.05	6.83

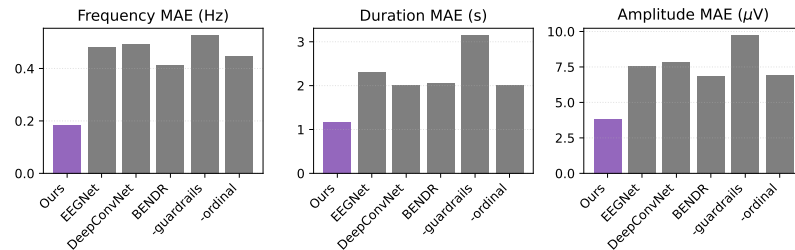


Figure 4: Performance on value extraction and localization tasks. (a) Value error distributions show measurement accuracy. (b) Localization accuracy across different spatial patterns.

pretraining on unlabeled corpora. The measurement-first paradigm generalizes beyond EEG to any high-frequency biosignal domain where precise quantitative values are as critical as descriptive text.

Ethics and deployment. We use publicly available, de-identified datasets (TUH, CHB-MIT) with IRB approval and HIPAA compliance. Clinical deployment requires local IRB approval, encrypted

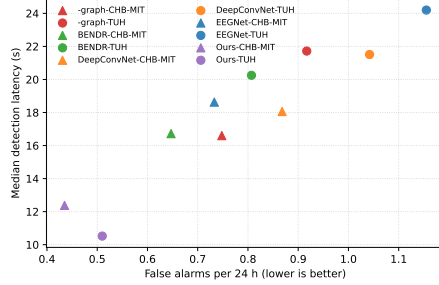


Figure 5: Detection trade-off: FA/24h vs. latency. Lower-left is better.

storage (HIPAA/GDPR), audit trails, patient consent, and human oversight. Our provenance tracking ensures every value is traceable for clinical and legal accountability^[29]. Beyond performance, structured reports with frozen measurements can assist clinical education by highlighting diagnostic features (3 Hz vs. 3.5 Hz spike-wave, focal vs. generalized spread, HFOs) and providing concrete scaffolds for learning electrophysiology.

8 Conclusion

We resolve the compression-precision paradox through a hybrid architecture separating measurement extraction from text generation. Signal processing extracts exact clinical values before neural compression, while language models compose narratives around frozen measurements. Evaluation on TUH and CHB-MIT datasets demonstrates substantial reductions in false alarms and detection latency while achieving measurement precision within clinical tolerance. This measurement-first paradigm generalizes to high-frequency biosignal domains requiring precise quantitative values alongside descriptive text, enabling trustworthy clinical decision support with full traceability.

References

- [1] World Health Organization. Epilepsy fact sheet, February 2024. URL <https://www.who.int/news-room/fact-sheets/detail/epilepsy>.
- [2] Jonathan W. Kim, Ahmed Alaa, and Danilo Bernardo. EEG-GPT: Exploring capabilities of large language models for EEG classification and interpretation. *arXiv preprint arXiv:2401.18006*, abs/2401.18006, 2024. URL <https://arxiv.org/abs/2401.18006>.
- [3] Demetres Kostas, Stephane Aroca-Ouellette, and Frank Rudzicz. BENDR: Using transformers and a contrastive self-supervised learning task to learn from massive amounts of EEG data. *Frontiers in Human Neuroscience*, 15:653659, 2021. doi: 10.3389/fnhum.2021.653659. URL <https://www.frontiersin.org/journals/human-neuroscience/articles/10.3389/fnhum.2021.653659/full>.
- [4] Jiyeon Lee, Gyeongmin Kim, and Kwanhyung Hong. Automated medical report generation for ECG data: Bridging medical text and signal processing with deep learning. *arXiv preprint arXiv:2412.04067*, abs/2412.04067, 2024. URL <https://arxiv.org/abs/2412.04067>.
- [5] Arthur C. Grant, Samah G. Abdel-Baki, Jeremy Weedon, Vanessa Arnedo, Geetha Chari, Ewa Koziorynska, Catherine Lushbough, Douglas Maus, Tresa McSween, Katherine A. Mortati, Alina Reznikov, and Ahmet Omurtag. EEG interpretation reliability and interpreter confidence: A large single-center study. *Epilepsy & Behavior*, 32:102–107, 2014. doi: 10.1016/j.yebeh.2014.01.011. URL <https://pubmed.ncbi.nlm.nih.gov/24531133/>.
- [6] Yuqi Chen, Kan Ren, Kaitao Song, Yansen Wang, Yifan Wang, Dongsheng Li, and Lili Qiu. EEGFormer: Towards transferable and interpretable large-scale EEG foundation model. *arXiv preprint arXiv:2401.10278*, abs/2401.10278, 2024. URL <https://arxiv.org/abs/2401.10278>.
- [7] Abdul Fatir Ansari, Oleksandr Shchur, Jaris Küken, Andreas Auer, Boran Han, Pedro Mercado, Syama Sundar Rangapuram, Huibin Shen, Lorenzo Stella, Ixiyan Zhang, Mononito Goswami, Shubham Kapoor, Danielle C. Maddix, Pablo Guerron, Tony Hu, Junming Yin, Nick Erickson, Prateek Mutalik Desai, Hao Wang, Huzefa Rangwala, George Karypis, Yuyang Wang, and Michael Bohlik-Schneider. Chronos-2: From univariate to universal forecasting. *arXiv preprint arXiv:2510.15821*, abs/2510.15821, 2025. URL <https://arxiv.org/abs/2510.15821>.
- [8] Yuqi Nie, Nam H Nguyen, Phanwadee Sinthong, and Jayant Kalagnanam. A time series is worth 64 words: Long-term forecasting with transformers. *arXiv preprint arXiv:2211.14730*, abs/2211.14730, 2023. URL <https://arxiv.org/abs/2211.14730>.
- [9] Abhijan Das, Weihao Kong, Andrew Leach, Shaan Mathur, Rajat Sen, and Rose Yu. A decoder-only foundation model for time-series forecasting. *arXiv preprint arXiv:2310.10688*, abs/2310.10688, 2024. URL <https://arxiv.org/abs/2310.10688>.
- [10] Zhihong Chen, Yan Song, Tsung-Hui Chang, and Xiang Wan. Generating radiology reports via memory-driven transformer. In *Proceedings of the 2020 Conference on Empirical Methods in Natural Language Processing (EMNLP)*, pages 1439–1449, Online, 2020. Association for Computational Linguistics. doi: 10.18653/v1/2020.emnlp-main.112. URL <https://aclanthology.org/2020.emnlp-main.112>.
- [11] Fenglin Liu, Xian Wu, Shen Ge, Wei Fan, and Yuexian Zou. Exploring and distilling posterior and prior knowledge for radiology report generation. In *Proceedings of the IEEE/CVF Conference on Computer Vision and Pattern Recognition*, pages 13753–13762, Virtual, 2021. IEEE. URL https://openaccess.thecvf.com/content/CVPR2021/papers/Liu_Exploring_and_Distilling_Posterior_and_Prior_Knowledge_for_Radiology_Report_CVPR_2021_paper.pdf.
- [12] Jing Wu, Yuli Wang, Zhengliang Zhong, et al. Vision-language foundation model for 3D medical imaging. *npj Artificial Intelligence*, 1:17, 2025. doi: 10.1038/s44387-025-00015-9. URL <https://www.nature.com/articles/s44387-025-00015-9>.
- [13] Nafatl Tishby and Noga Zaslavsky. Deep learning and the information bottleneck principle. In *2015 IEEE Information Theory Workshop (ITW)*, pages 1–5, Jerusalem, Israel, 2015. IEEE. doi: 10.1109/ITW.2015.7133169. URL <https://ieeexplore.ieee.org/document/7133169>.
- [14] U.S. Food and Drug Administration. Clinical decision support software: Guidance for industry and food and drug administration staff, 2022. URL <https://www.fda.gov/regulatory-information/search-fda-guidance-documents/clinical-decision-support-software>.
- [15] Xiaosong Li, Yueming Zhou, Nicha Dvornek, Meiyi Zhang, and James Duncan. Graph-informed neural networks for spatial and temporal modeling of EEG signals in seizure detection. *IEEE Transactions on Neural Systems and Rehabilitation Engineering*, 31:2154–2163, 2023.
- [16] Albert Gu, Karan Goel, and Christopher Ré. Efficiently modeling long sequences with structured state spaces. In *International Conference on Learning Representations*, Virtual, 2022. OpenReview.net. URL <https://arxiv.org/abs/2111.00396>.
- [17] Albert Gu and Tri Dao. Mamba: Linear-time sequence modeling with selective state spaces. *arXiv preprint arXiv:2312.00752*, abs/2312.00752, 2024. URL <https://arxiv.org/abs/2312.00752>.
- [18] Aaron van den Oord, Yazhe Li, and Oriol Vinyals. Representation learning with contrastive predictive coding. *arXiv preprint arXiv:1807.03748*, abs/1807.03748, 2018. URL <https://arxiv.org/abs/1807.03748>.
- [19] Alex Radford, Joon Woo Kim, Chris Hallacy, Aditya Ramesh, Gabriel Goh, Sandhini Agarwal, Girish Sastry, Amanda Askell, Pamela Mishkin, Jack Clark, et al. Learning transferable visual models from natural language supervision. In *International Conference on Machine Learning*, pages 8748–8763, Virtual, 2021. PMLR. URL <https://arxiv.org/abs/2103.00020>.
- [20] Ignacio Diaz, Manuel J. Marin-Jimenez, and Fernando de la Torre. Soft labels for ordinal regression. In *IEEE/CVF Conference on Computer Vision and Pattern Recognition*, pages 4738–4747, Long Beach, CA, USA, 2019. IEEE. URL https://openaccess.thecvf.com/content_CVPR_2019/papers/Diaz_Soft_Labels_for_Ordinal_Regression_CVPR_2019_paper.pdf.
- [21] Michaël Perrot and Zaid Harchaoui. The earth mover’s pinball loss: Quantiles for histogram-valued regression. *arXiv preprint arXiv:2106.02051*, abs/2106.02051, 2021. URL <https://arxiv.org/abs/2106.02051>.
- [22] Chen Xu and Yao Xie. Conformal time-series forecasting. In *Advances in Neural Information Processing Systems*, pages 11865–11877, Virtual, 2021. Curran Associates, Inc. URL <https://proceedings.neurips.cc/paper/2021/file/312f1ba2a72318eda995a67835fad5-Paper.pdf>.
- [23] Edward J. Hu, Yelong Shen, Phillip Wallis, Zeyuan Allen-Zhu, Yuanzhi Li, Shean Wang, Lu Wang, and Weizhu Chen. LoRA: Low-rank adaptation of large language models. In *International Conference on Learning Representations*, Virtual, 2022. OpenReview.net. URL <https://arxiv.org/abs/2106.09685>.
- [24] Iyad Obeid and Joseph Picone. The temple university hospital EEG data corpus. *Frontiers in Neuroscience*, 10:196, 2016. doi: 10.3389/fnins.2016.00196. URL <https://www.frontiersin.org/journals/neuroscience/articles/10.3389/fnins.2016.00196/full>.
- [25] Vinit Shah, Eva von Weltin, Silvia Lopez, James R. McHugh, Lydia Veloso, Meysam Golmohammadi, Iyad Obeid, and Joseph Picone. The temple university hospital seizure detection corpus. *Frontiers in Neuroinformatics*, 12:83, 2018. doi: 10.3389/fninf.2018.00083. URL <https://www.frontiersin.org/journals/neuroinformatics/articles/10.3389/fninf.2018.00083/full>.

- [26] Ali Shoeb and John Guttag. Application of machine learning to epileptic seizure detection. In *Proceedings of the 27th International Conference on Machine Learning (ICML)*, pages 975–982, Haifa, Israel, 2010. Omnipress. URL <https://physionet.org/content/chbmit/1.0.0/>.
- [27] Vernon J. Lawhern, Amelia J. Solon, Nicholas R. Waytowich, Stephen M. Gordon, Chou P. Hung, and Brent J. Lance. EEGNet: a compact convolutional neural network for EEG-based brain–computer interfaces. *Journal of Neural Engineering*, 15(5):056013, 2018. doi: 10.1088/1741-2552/aace8c. URL <https://pubmed.ncbi.nlm.nih.gov/29932424/>.
- [28] Robin T. Schirrmeister, Jost T. Springenberg, Lukas D. J. Fiederer, Martin Glasstetter, Katharina Eggensperger, Michael Tangermann, Frank Hutter, Wolfram Burgard, and Tonio Ball. Deep learning with convolutional neural networks for EEG decoding and visualization. *Human Brain Mapping*, 38(11):5391–5420, 2017. doi: 10.1002/hbm.23730. URL <https://pubmed.ncbi.nlm.nih.gov/28782865/>.
- [29] Boris Baćić, Claudiu Vasile, Chengwei Feng, and Marian G. Ciucă. Towards nationwide analytical healthcare infrastructures: A privacy-preserving augmented knee rehabilitation case study. *arXiv preprint arXiv:2412.20733*, abs/2412.20733, 2024. URL <https://arxiv.org/abs/2412.20733>.